Optics and Laser Technology 112 (2019) 215–221

Contents lists available at ScienceDirect

Optics and Laser Technology

journal homepage: www.elsevier.com/locate/optlastec

Full length article

Tunable terahertz metamaterial by using three-dimensional double split-ring resonators

Yu-Sheng Lin*,†, Shaoquan Liao†, Xiaoyan Liu, Yanlin Tong, Zefeng Xu, Ruijia Xu, Dongyuan Yao, Yangbin Yu

State Key Laboratory of Optoelectronic Materials and Technologies, School of Electronics and Information Technology, Sun Yat-Sen University, Guangzhou 510275, China

HIGHLIGHTS

- Tunable single-band and dual-band resonances.
- The maximum tuning range of dual-band resonance is 0.55 THz.
- Free spectrum range (FSR) can be tuned from 0.20 THz to 0.75 THz.
- Tunable and switchable single-band and dual-band resonances.
- High stability to allow manufacturing tolerance for widespread applications.

ARTICLE INFO

Keywords:
Metamaterial
THz modulator
THz resonator

ABSTRACT

We present an optically tunable terahertz (THz) metamaterial by using three-dimensional double split-ring resonators (3D-DSRR), which shows superior properties in adjustability. They exhibit tunable single-band and dual-band resonances by changing height between inner and outer SRRs. The maximum tuning range of dual-band resonance is 0.55 THz from the resonance of 0.45 THz shifted to the resonance of 1.00 THz. The corresponding tuning range of free spectrum range (FSR) spanned two resonances can be tuned from 0.20 THz to 0.75 THz. By changing radius of inner SRR from 14.5 μm to 22.5 μm, the tuning range of resonance is 0.40 THz. While changing the height between inner and outer SRRs and kept the radiuses of inner and outer SRRs as constant as 22.5 μm, 3D-DSRR can be tuned to have two resonances and then merge into one resonance. 3D-DSRR shows a tunable and switchable resonance for single-band and dual-band characteristics. These characterizations are very suitable for the use of tunable multi-resonance applications. To further investigate the stability of 3D-DSRR, the rotation angles of inner and outer SRRs are modified from 0° to 180°, respectively. The corresponding resonances are identical. Such results indicate the proposed device with high stability to allow manufacturing tolerance and potentially to be used in wearable electronic devices, pressure sensors, and other fields.

1. Introduction

Metamaterials are artificial electromagnetic structures that cannot found in nature, which show many unique electric and magnetic characteristics, such as artificial magnetism [1], toroidal response [2], field enhancement [3,4], subwavelength imaging [5], negative refraction index [6], and so on. By tailoring suitable metamaterials, they can be operated in visible [7,8], infrared (IR) [9,10], and terahertz (THz) [11–13] spectrum ranges. Among of these spectra, THz metamaterial is an emerging field that metamaterial has a great electromagnetic response in THz frequencies. To increase the interaction of the THz wave with the sample, research has been carried out in this field to characterize how these THz waves interact with shape and size of designed metamaterial patterns. Therefore, the electromagnetic characteristics of metamaterials can be controlled and manipulated to be used in widespread applications, such as filters [14], super lenses [15], invisibility cloaks [16], perfect absorbers [17], and sensors [18].

The classic THz metamaterial design is considered as a ring with a common split, i.e. split-ring resonator (SRR), which was first theoretically proposed in 1999 and then experimentally verified in 2000

* Corresponding author.
E-mail address: linyoush@mail.sysu.edu.cn (Y.-S. Lin).
† These authors contributed equally.

https://doi.org/10.1016/j.optlastec.2018.11.020
Received 22 July 2018; Received in revised form 28 September 2018; Accepted 10 November 2018
Available online 22 November 2018
0030-3992/

[19,20]. Afterwards, some derivative designs such as U-shaped SRR [21], complementary SRR (cSRR) [22], I-shaped SRR [23], V-shaped SRR [24], electric SRR (eSRR) [25,26], and three-dimensional (3D) SRR [27,28] are presented and demonstrated. However, the resonant frequencies of these designs are unaltered, which can only filter or absorb certain electromagnetic spectra passively. To improve the flexibility of THz metamaterial, there are literatures reported the tuning mechanisms, such as thermal annealing [29–31], ferroelectric materials [32,33], semiconductor materials or diodes [34], laser pumping [35], liquid crystal [36], electrostatic force [37] and so on. In these tuning approaches, reconfigurable metamaterials become feasible in many applications, which are other than the use of liquid crystal, ferroelectric materials, and semiconductor diodes are highly dependent on the nonlinear properties of the nature material. These methods suffer from a limited tuning range [21].

In this study, we propose and investigate 3D double SRR (3D-DSRR) in THz frequency range. 3D-DSRR is composed of inner and outer SRRs with a height between them on Si substrate. Owing to metamaterial geometry has enormous implications to electromagnetic response, we will compare and discuss the geometrical dimensions of metamaterial, including the height between inner and outer SRRs, radius of inner SRR, rotation angles of inner and outer SRRs. Such optically tunable THz metamaterial by using 3D-DSRR shows superior properties in adjustability. They exhibit tunable and switchable single-band and dual-band resonance by changing height of inner and outer SRRs. These characterizations are very suitable for the use of tunable multi-resonance applications. To further investigate the stability of 3D-DSRR, the relationships of rotation angle of inner and outer SRRs from 0° to 180° are compared and discussed. Such optical properties of 3D-DSRR open an avenue to be used in widespread applications with high portability, flexibility, and compatibility.

2. Materials and methods

Fig. 1(a) shows the schematic drawing of 3D-DSRR which is composed of two Au concentric split-rings with 200 nm in thickness on Si substrate. The 3D-DSRR array as well as the coordinates of incident electromagnetic wave are shown in Fig. 1(a), where *E*, *H*, and *k* are the electric field, magnetic field, and Poynting vector of electromagnetic wave, respectively. The denotations of 3D-DSRR unit cell are indicated as shown in Fig. 1(b). They are period of 3D-DSRR ($p_x \times p_y$), outer radius of 3D-DSRR (r_1), inner radius of 3D-DSRR (r_2), line width of 3D-DSRR (w), and gap of split (g), where p_x, p_y, r_1, w, and g are kept as constant as 50 μm, 50 μm, 22.5 μm, 4 μm, and 4 μm, respectively. In this study, the outer and inner radiuses of 3D-DSRR are firstly kept at r_1 = 22.5 μm and r_2 = 14.5 μm to investigate the electromagnetic responses by changing height (h) between outer and inner SRRs of 3D-DSRR. Secondly, the relationships of h, r_1 and r_2 parameters will be compared and discussed to figure out the optimized geometrical parameters of 3D-DSRR. Thirdly, h parameter will be investigated under the condition of the same SRR radius ($r_1 = r_2$ = 22.5 μm) to make the device with flexible tunability. Finally, the influence of rotation angles of outer and inner SRRs will be discussed and compared.

3. Results and discussions

The reflectivity of electromagnetic wave can be expressed by Eq. (1), where n_0 is refraction index of air, n_s is refraction index of Si substrate, and n_{EM} is refraction index of electromagnetic radiation.

$$R = 1 - \frac{4n_0 n_s n_{EM}^2}{(n_0 n_s + n_{EM}^2)^2} = \left[\frac{n_0 n_s - n_{EM}^2}{n_0 n_s + n_{EM}^2}\right]^2 \quad (1)$$

where n_{EM} equals $\sqrt{\varepsilon(\omega)\mu(\omega)}$. The resonant frequency of 3D-DSRR is a function of n_{EM}, which is a harmonic oscillator to an external frequency-dependent perturbation expressed by

$$\varepsilon(\omega) = 1 - \frac{F \bullet \omega_{pe}^2}{\omega^2 - \omega_{LCe}^2} \quad (2)$$

$$\mu(\omega) = 1 - \frac{F \bullet \omega_{pm}^2}{\omega^2 - \omega_{LCm}^2} \quad (3)$$

where ω_p is plasma frequency, ω_{LC} is resonant frequency, and F is a dimensionless quantity, while subscripts e and m refer to electric and magnetic response [38].

Fig. 2 shows the reflection spectra of 3D-DSRR by changing h parameter from 0 μm to 10 μm with constant parameters of r_1 = 22.5 μm and r_2 = 14.5 μm. There are two resonances at the condition of h = 0 μm as the black curve shown in Fig. 2(a), which are 0.25 THz and 0.45 THz, respectively. By increasing h from 0 μm to 3.8 μm, the first resonance (0.25 THz) is kept as constant and the second resonance (0.45 THz) will be blue-shift to 1.00 THz. The tuning range is 0.55 THz. The corresponding free spectrum range (FSR) is defined as the bandwidth of first and second resonances, which tuning range of FSR can be tuned from 0.20 THz to 0.75 THz. When further increasing h from 3.8 μm to 4 μm, the second resonance will be returned back to 0.45 THz. It is a red-shift of 0.55 THz, while the first resonance is still as constant. Continuously increasing h from 4 μm to 10 μm, the first resonance is also identical and second resonance is a little variation in the range of 0.05 THz. Therefore, it is almost the same electromagnetic response for 3D-DSRR with different h value in the range of 4 μm and 10 μm. The relationship of second resonance and h value is summarized in Fig. 2(c). It indicates the tendency is firstly increasing and then sharply decreasing to keep as constant. These results show the proposed 3D-DSRR can be tuned with a tuning range of 0.55 THz by changing h parameter in the range of 0 μm to 3.8 μm.

To investigate the relationships of electromagnetic responses of 3D-DSRR with different r_2 and h, r_2 values are modified from 14.5 μm to

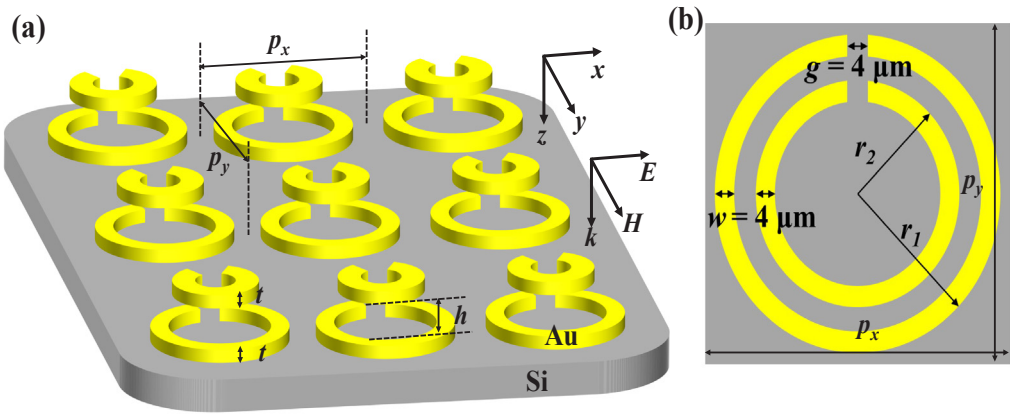

Fig. 1. Schematic drawings of (a) 3D-view and (b) unit cell of 3D-DSRR. The coordinates of incident electromagnetic wave are shown in (a), where *E*, *H*, and *k* are the electric field, magnetic field, and Poynting vector of electromagnetic wave, respectively. The period, outer radius, inner radius, line width of 3D-DSRR, and gap of split are denoted as p_x, p_y, r_1, r_2, w, and g, respectively.

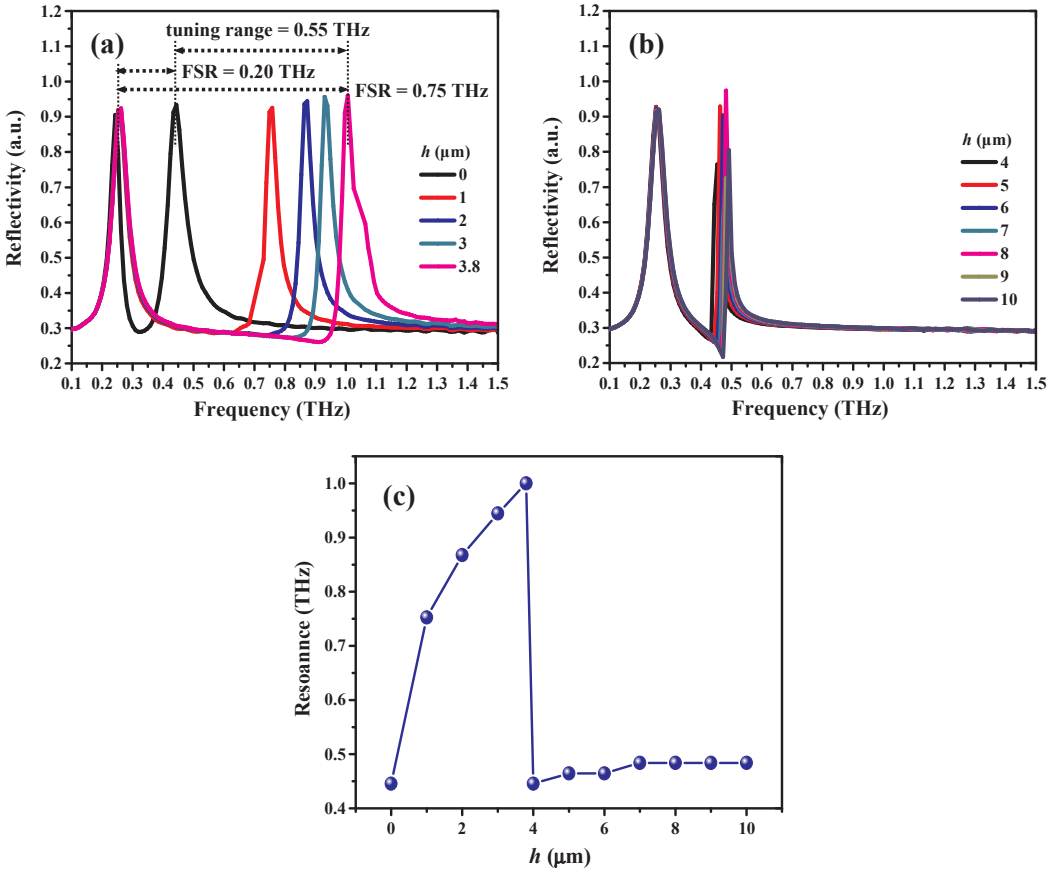

Fig. 2. (a) Reflection spectra of 3D-DSRR by changing h parameter from 0 μm to 3.8 μm. (b) Reflection spectra of 3D-DSRR by changing h parameter from 4 μm to 10 μm. (c) The relationship of resonance and h parameter.

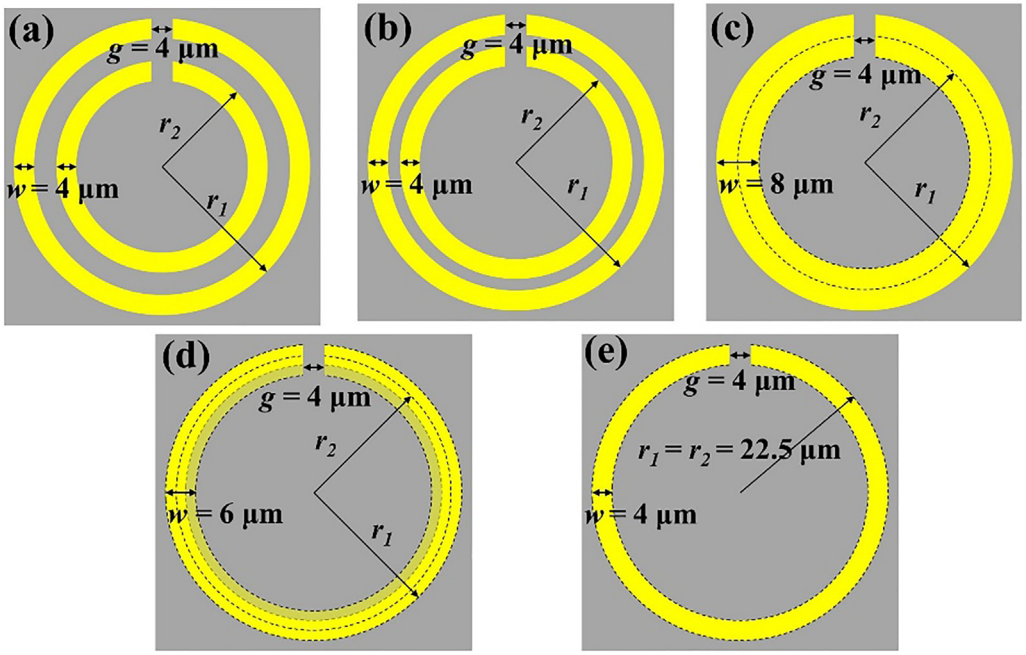

Fig. 3. Illustrations of 3D-DSRR with radius variation of inner SRR (r_2). (a) r_2 = 14.5 μm, (b) r_2 = 16.5 μm, (c) r_2 = 18.5 μm, (d) r_2 = 20.5 μm, and (e) r_2 = 22.5 μm, respectively.

22.5 μm and h value is modified from 2 μm to 6 μm. The corresponding top-view schematics are illustrated in Fig. 3. The parameters r_1 and g are kept as constant as 22.5 μm and 4 μm, respectively, while r_2 values are 14.5 μm (Fig. 3(a)), 16.5 μm (Fig. 3(b)), 18.5 μm (Fig. 3(c)), 20.5 μm (Fig. 3(d)), 22.5 μm (Fig. 3(e)), respectively. The reflection spectra of 3D-DSRR with different r_2 and h are shown in Fig. 4. The first

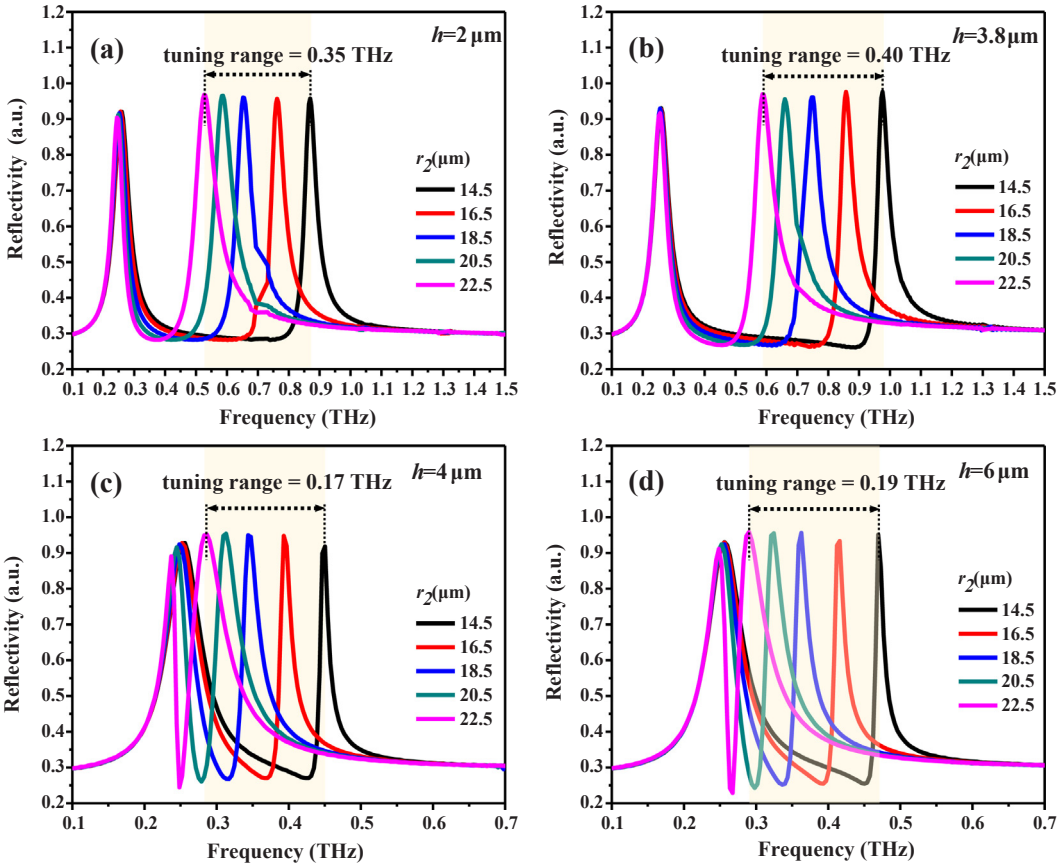

Fig. 4. Reflection spectra of 3D-DSRR with different r_2 parameter under the condition of (a) h = 2 μm, (b) h = 3.8 μm, (c) h = 4 μm, (d) h = 6 μm, respectively.

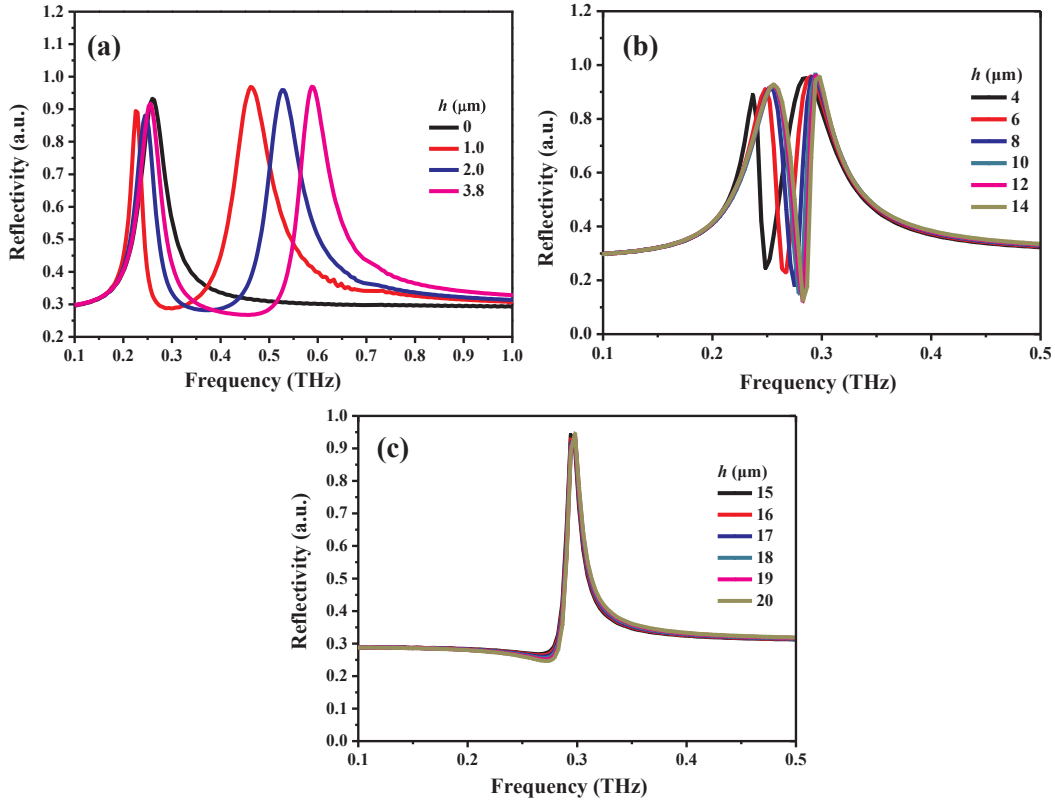

Fig. 5. Reflection spectra of 3D-DSRR with the same radius of inner and outer SRR (r_1 = r_2 = 22.5 μm) by changing h parameter. (a) h is in the range of 0 μm to 3.8 μm; (b) h is in the range of 4–14 μm; (c) h is in the range of 15–20 μm, respectively.

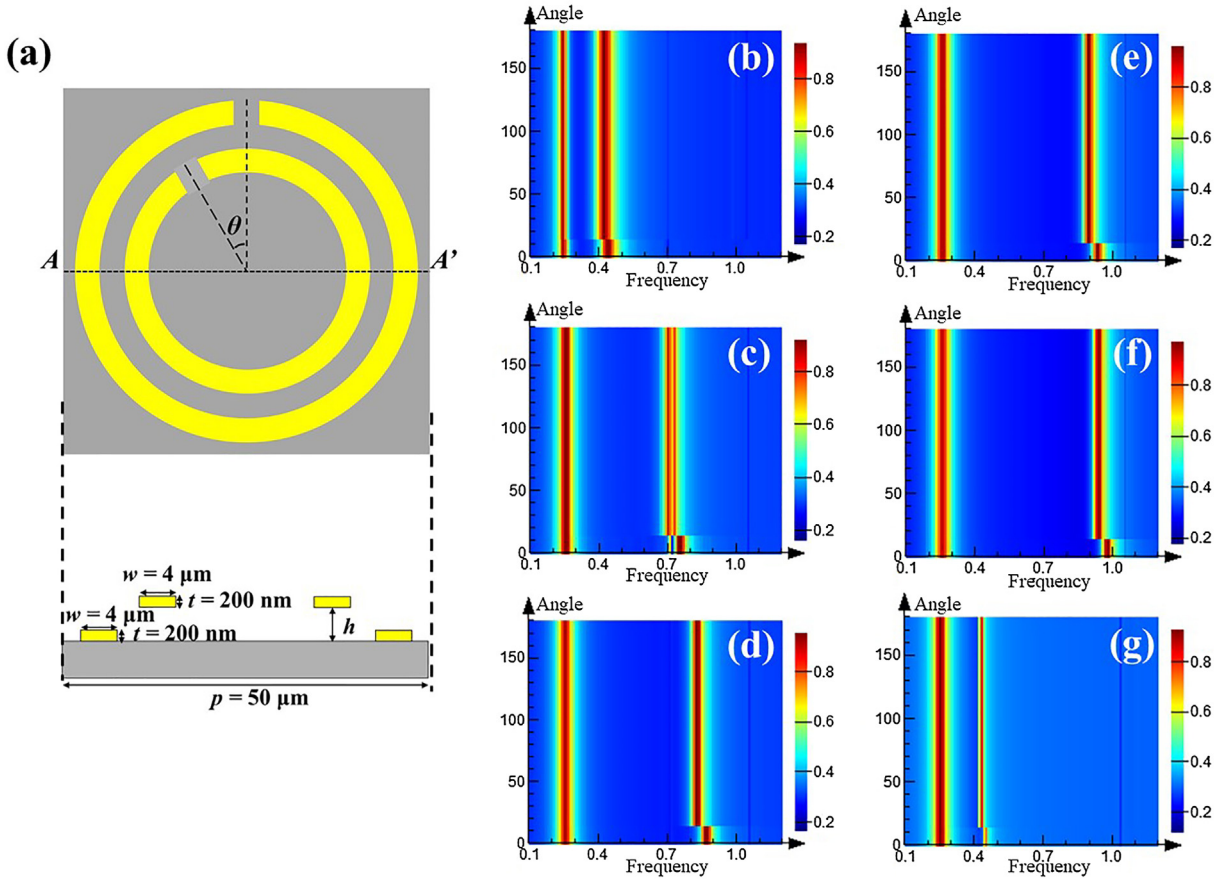

Fig. 6. (a) Schematic drawing of 3D-DSRR by changing rotation angle of inner SRR from 0° to 180°. The bottom drawing is the cross-sectional view along AA′ line. (b–g) are the relationship of resonance and rotation angle with (b) h = 0 μm, (c) h = 1 μm, (d) h = 2 μm, (e) h = 3 μm, (f) h = 3.8 μm, (g) h = 4 μm, respectively.

resonances are kept as constant at 0.25 THz and second resonances have red-shifts of 0.35 THz, 0.40 THz, 0.17 THz, and 0.17 THz by changing r_2 from 14.5 μm to 22.5 μm for h = 2 μm, 3.8 μm, 4 μm, and 6 μm, respectively, as shown in Fig. 4(a–d). The results indicate the first resonance of 3D-DSRR can be kept as constant and the second resonance of 3D-DSRR is tunable by changing r_2. The maximum tuning range is 0.40 THz.

Fig. 5 shows the reflection spectra of 3D-DSRR with the same SRRs by changing h. The radiuses of inner and outer SRRs are kept as 22.5 μm. In Fig. 5(a), there are two resonances at the condition of h = 2 μm and h = 3.8 μm. By increasing h value to 3.8 μm, the first resonance is almost kept as constant at 0.25 THz and the second resonance is blue-shift to 0.60 THz. The maximum FSR is 0.35 THz for 3D-DSRR with h = 3.8 μm. When h is continuously increased to the range of 4–14 μm, two resonances becomes close at 0.25 THz and 0.30 THz, respectively, and keeps as constant as shown in Fig. 5(b). The FSR is 0.05 THz. It means the electromagnetic response of device is resistant to the change of h in the range of 4 μm to 14 μm. It is clearly observed two resonances will merge together at 0.30 THz when h is increased over 15 μm as shown in Fig. 5(c). Regarding to the results of Fig. 5, 3D-DSRR can be tuned to possess two resonances and then merge into one resonance, which is tunable resonance for single-band and dual-band. These characterizations are very suitable for the use of tunable multi-resonance applications.

To further investigate the stability of 3D-DSRR, the influence of rotation angle of inner and outer SRRs to reflection spectra are discussed. Figs. 6 and 7 show the results of 3D-DSRR with the rotation angle from 0° to 180° of inner and outer SRRs, respectively, by changing different h value from 0 μm to 4 μm. Fig.s 6(a) and 7(a) show the top-view schematics of 3D-DSRR with a rotation angle of inner and outer SRRs, respectively. The corresponding cross-sectional schematics along AA′ lines are indicated the geometrical parameters of 3D-DSRR as shown in the bottom drawings of Figs. 6(a) and 7(a) with constant parameters of r_1 = 22.5 μm and r_2 = 14.5 μm. The rotation angle is defined as the angle between center line of these two SRR's gap. Figs. 6(b–g) and 7(b–g) are the relationships of resonance and rotation angle with different h value. They are h = 0 μm (Figs. 6(b) and 7(b)), h = 1 μm (Figs. 6(c) and 7(c)), h = 2 μm (Figs. 6(d) and 7(d)), h = 3 μm (Figs. 6(e) and 7(e)), h = 3.8 μm (Figs. 6(f) and 7(f)), h = 4 μm (Figs. 6(g) and 7(g)), respectively. The results indicate the first resonance for inner SRR with a rotation angle by changing h value kept as a constant at 0.25 THz, while the corresponding second resonance is blue-shift from 0.43 THz to 0.95 THz. The tuning range of second resonance is 0.52 THz. It is clearly observed that 3D-DSRR exhibits angle-independence and the electromagnetic response is resistant to the rotation angle of inner and outer SRRs. It means the permissible tolerances of rotation angle is 360° for the changing of h value from 0 μm to 4 μm. By pressing the inner SRR, the height between inner and outer SRRs (h) can be modified and then tuned the electromagnetic response of device even twisted the inner SRR to have a rotation angle in operation. The electromagnetic response is kept as constant. Such results are very suitable for the use of pressure sensor. Furthermore, the proposed device can be fabricated on flexible substrate, such as polydimethylsiloxane (PDMS), polyimide (PI), polyethylene terephthalate (PET), polyethylene naphthalene (PEN) to perform the deformable electronic devices.

In the future work, we will design and demonstrate 3D-DSRR by using micro-electro-mechanical systems (MEMS) technology to realize THz pressure sensor and flexible electronic device. The schematic drawing of proposed device is shown in Fig. 8(a). To realize the 3D-

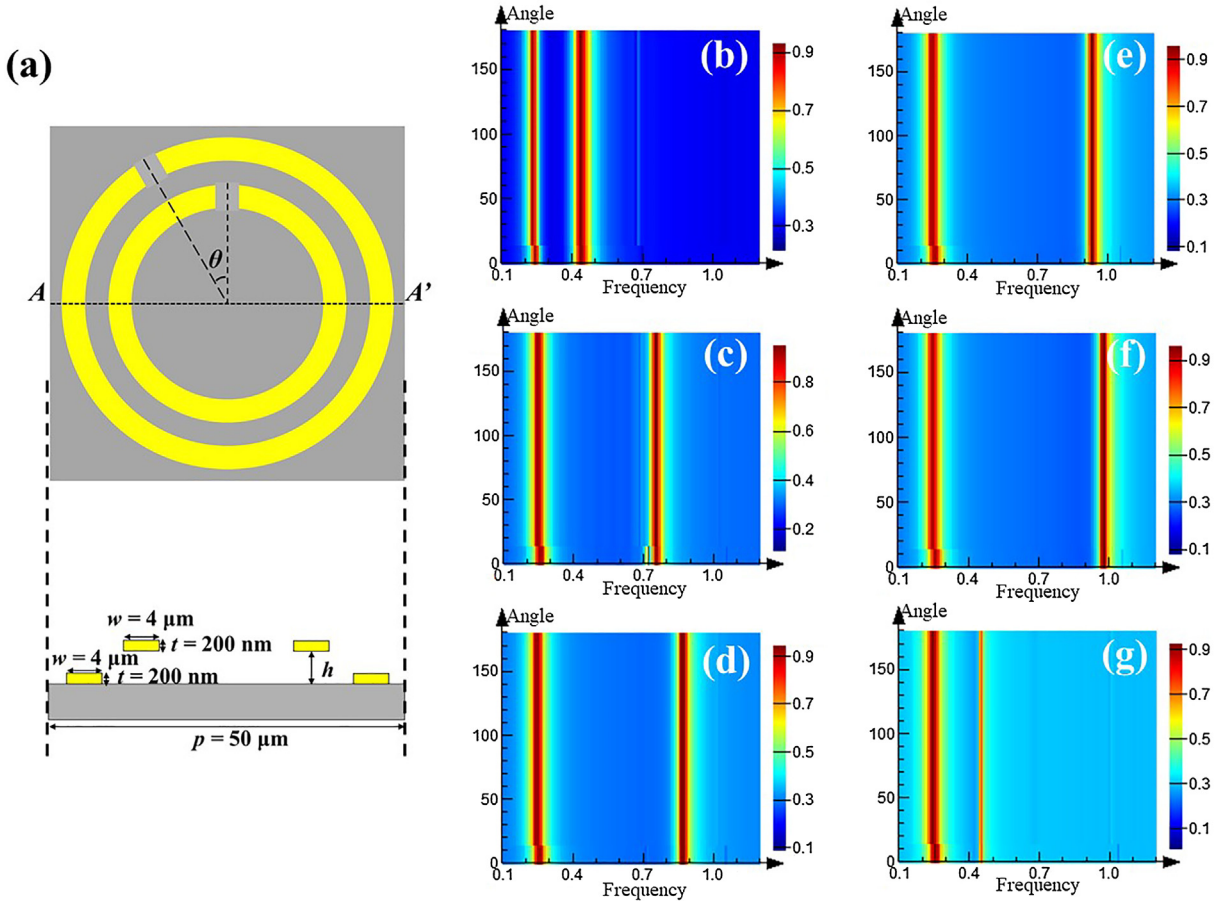

Fig. 7. (a) Schematic drawing of 3D-DSRR by changing rotation angle of outer SRR from 0° to 180°. The bottom drawing is the cross-sectional view along AA′ line. (b–g) are the relationship of resonance and rotation angle with (b) h = 0 μm, (c) h = 1 μm, (d) h = 2 μm, (e) h = 3 μm, (f) h = 3.8 μm, (g) h = 4 μm, respectively.

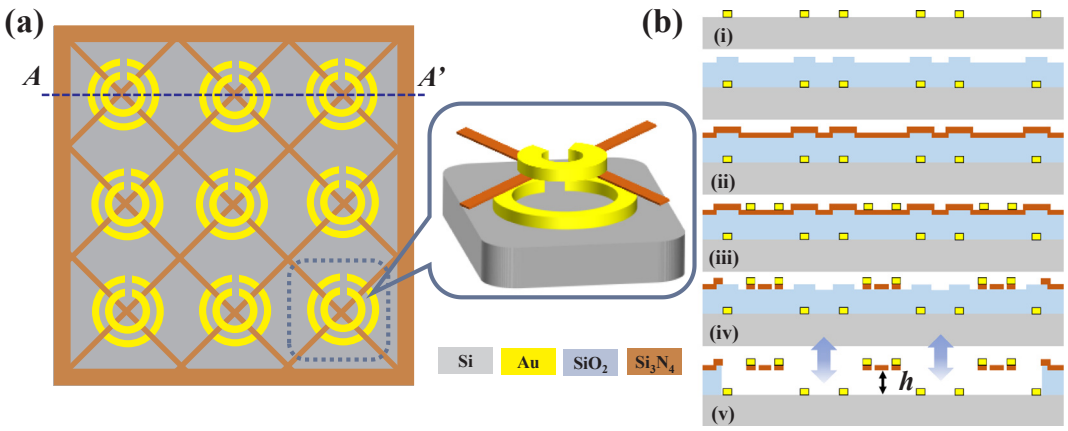

Fig. 8. (a) Schematic drawing of proposed 3D-DSRR for pressure sensor application. (b) Fabrication process flow of proposed 3D-DSRR along AA′ line in (a). (i) The deposition of Au thin-film with 200 nm in thickness for outer ring of 3D-DSRR by using lift-off process. (ii) The depositions of SiO_2 and Si_3N_4 thin-films by using PECVD sequentially. (iii) The deposition of Au thin-film with 200 nm in thickness for inner ring of 3D-DSRR by using lift-off process. (iv) Si_3N_4 thin-film is patterned by using RIE processes. (v) The microstructures are released by using vapor HF.

DSRR to be used in pressure sensor, the inner ring of device is suspended and supported by using a Si_3N_4 membrane with microstructures. The reason for the use of Si_3N_4 membrane is very low absorption coefficient of Si_3N_4 in THz frequency range [39]. That can be ignored the influence of electromagnetic wave propagation in the reflection spectra of 3D-DSRR. The proposed fabrication process of tunable 3D-DSRR is illustrated in Fig. 8(b). First, an Au thin-film with 200 nm in thickness for outer ring of 3D-DSRR is deposited by using lift-off process as shown in Fig. 8(b-i). Second, SiO_2 and Si_3N_4 thin-films are deposited by using plasma enhanced chemical vapor deposition (PECVD) process as shown in Fig. 8(b-ii). Third, an Au thin-film with 200 nm in thickness for inner ring of 3D-DSRR is deposited by using lift-off process as shown in Fig. 8(b-iii). Fourth, the Si_3N_4 thin-film is patterned by using reactive ion etching (RIE) process as shown in Fig. 8(b-iv). Finally, the microstructures are released by using vapor HF to perform the inner ring of device suspended and supported by Si_3N_4 membrane as shown in Fig. 8(b-v). Therefore, such device can be tuned the height between inner and outer rings of 3D-DSRR to make the

resonance shift and then to have potentially used in pressure sensor application.

4. Conclusions

In conclusion, we present a tunable 3D-DSRR by modifying the relative geometrical dimensions to investigate superior optical properties in THz frequency range. 3D-DSRR exhibits two resonances caused from inner and outer SRR, respectively. The first resonance is kept as constant and the second resonance can be tuned to have a tuning range of 0.55 THz. The corresponding tuning range of FSR is from 0.20 THz to 0.75 THz. Furthermore, the proposed 3D-DSRR can be modified to have single-band and dual-band resonances by changing the height between inner and outer SRRs. To investigate the stability of 3D-DSRR, the changes of rotation angle of inner and outer SRRs from 0° to 180° are constant, which means the electromagnetic response of 3D-DSRR is resistant to the rotation angle of inner and outer SRRs owing to the symmetrical structures of DSRR. This work provides the detail investigation of geometrical parameters for tunable 3D-DSRR. With the investigation of geometrical relationships of 3D-DSRR being fully understood, the design of 3D-DSRR provides a new direction for future designs of optical applications. As an advantage over planar DSRR, 3D-DSRR device is capable of continuous tuning by changing the height between inner and outer rings of 3D-DSRR. This promises future tunable THz designs based on pressing inner ring microstructures only. These results pave a way for the use of 3D-DSRR in wearable electronic devices, pressure sensors, tunable filters, and other applications.

Acknowledgement

The authors acknowledge the financial support from research grants of 100 Talents Program of Sun Yat-Sen University (grant number 76120-18831103) and the State Key Laboratory of Optoelectronic Materials and Technologies of Sun Yat-Sen University for the use of experimental equipment.

Appendix A. Supplementary material

Supplementary data to this article can be found online at https://doi.org/10.1016/j.optlastec.2018.11.020.

References

[1] S. Lannebère, S. Campione, A. Aradian, M. Albani, F. Capolino, Artificial magnetism at terahertz frequencies from three-dimensional lattices of TiO2 microspheres accounting for spatial dispersion and magnetoelectric coupling, Opt. Soc. Am. B 31 (2014) 1078–1086.
[2] I.V. Stenishchev, A.A. Basharinl, Toroidal response in all-dielectric metamaterials based on water, Sci. Rep. 7 (2017) 9468.
[3] M. Kozina, M. Pancaldi, C. Bernhard, T.V. Driel, J.M. Glownia, P. Marsik, M. Radovic, C.A.F. Vaz, D. Zhu, S. Bonetti, U. Staub, M.C. Hoffmann, Local terahertz field enhancement for time-resolved X-ray diffraction, Appl. Phys. Lett. 110 (2017) 081106.
[4] S.P. Zhan, X.F. Wu, C. Tan, J. Xiong, S.G. Hu, J.S. Hu, S.B. Wu, Y.Y. Gao, Y.X. Liu, Enhanced upconversion based on the ultrahigh local field enhancement in a multilayered UCNPs-metamaterial composite system, J. Alloy Com. 735 (2018) 372–376.
[5] J.F. Federici, B. Schulkin, F. Huang, D. Gary, R. Barat, F. Oliveira, D. Zimdars, THz imaging and sensing for security applications-explosives, weapons and drugs, Sem. Sci. Tech. 20 (2005) S266–S280.
[6] Z.J. Wong, Y. Wang, K. O'Brien, J. Rho, X.B. Yin, S. Zhang, N. Fang, T. Yen, X. Zhang, Optical and acoustic metamaterials: superlens, negative refractive index and invisibility cloak, J. Opt. 19 (2017) 084007.
[7] D. Wu, R.F. Li, Y.M. Liu, Z.Y. Yu, L. Yu, L. Chen, C. Liu, R. Ma, H. Ye, Ultra-narrow band perfect absorber and its application as plasmonic sensor in the visible region, Nano Res. Lett. 12 (2017) 427.
[8] Y.S. Lin, W. Chen, Perfect meta-absorber by using pod-like nanostructures with ultra-broadband, omnidirectional, and polarization-independent characteristics, Sci. Rep. 8 (2018) 7150.
[9] R. Xu, Y.S. Lin, Characterizations of reconfigurable infrared metamaterial absorbers, Opt. Lett. 43 (2018) 4783–4786.
[10] R. Xu, J. Luo, J. Sha, J. Zhong, Z. Xu, Y. Tong, Y.S. Lin, Stretchable IR metamaterial with ultra-narrowband perfect absorption, Appl. Phys. Lett. 113 (2018) 101907.
[11] H. Tao, A.C. Strikwerda, K. Fan, W.J. Padilla, X. Zhang, R.D. Averitt, MEMS based structurally tunable metamaterials at terahertz frequencies, J. Infrared Millim. Terahertz Waves 32 (2011) 580–595.
[12] D. Yao, K. Yan, X. Liu, S. Liao, Y. Yu, Y.S. Lin, Tunable terahertz metamaterial by using asymmetrical double split-ring resonators (ADSRRs), OSA Contin. 1 (2018) 349–357.
[13] X.G. Zhao, K.B. Fan, J.D. Zhang, G.R. Keiser, G.W. Duan, R.D. Averitt, X. Zhang, Voltage-tunable dual-layer terahertz metamaterials, Microsyst. Nanoeng. 2 (2016) 16025.
[14] Y.S. Lin, W.J. Chen, A large-area, wide-incident-angle, and polarization-independent plasmonic color filter for glucose sensing, Opt. Mater. 75 (2018) 739–743.
[15] M. Chen, H. Jiang, H. Zhang, D.S. Li, Y.R. Wang, Design of an acoustic superlens using single-phase metamaterials with a star-shaped lattice structure, Sci. Rep. 8 (2018) 1861.
[16] M.M. Behbahani, E. Amooghorban, A. Mahdifar, Spontaneous emission and the operation of invisibility cloaks, Phys. Rev. A 94 (2016) 013854.
[17] H.C. Yu, Z.Y. Zhao, Q.B. Qian, J. Xu, P. Gou, Y.X. Zou, J. Cao, L. Yang, J. Qian, Z.H. An, Metamaterial perfect absorbers with solid and inverse periodic cross structures for optoelectronic applications, Opt. Exp. 25 (2017) 8288–8295.
[18] W. Wang, F.P. Yan, S.Y. Tan, H. Zhou, Y.F. Hou, Ultrasensitive terahertz metamaterial sensor based on vertical split ring resonators, Photon. Res. 5 (2017) 571–577.
[19] L.A. Coldren, Monolithic tunable diode lasers, IEEE J. Sel. Top. Quant. Electron. 6 (2000) 988–999.
[20] D.R. Smith, W.J. Padilla, D.C. Vier, S.C. Nemat-Nasser, S. Schultz, Composite medium with simultaneously negative permeability and permittivity, Phys. Rev. Lett. 84 (2000) 4184–4187.
[21] Y.S. Lin, C.Y. Huang, C. Lee, Reconfiguration of resonance characteristics for terahertz U-shape metamaterial using MEMS mechanism, IEEE J. Sel. Top. Quant. Electron. 21 (2015) 2700207.
[22] F. Lan, Z.Q. Yang, L.M. Qi, X. Gao, Z.J. Shi, Terahertz dual-resonance bandpass filter using bilayer reformative complementary metamaterial structures, Opt. Lett. 39 (2014) 1709–1712.
[23] W.Q. Cao, B.N. Zhang, A.J. Liu, T.B. Yu, D.S. Guo, Y. Wei, Broadband high-gain periodic endfire antenna by using I-shaped resonator (ISR) structures, IEEE Antennas Wirel. Propag. Lett. 11 (2012) 1470–1473.
[24] K. Kishor, M.N. Baitha, R.K. Sinha, B. Lahiri, Tunable negative refractive index metamaterial from V-shaped SRR structure: fabrication and characterization, J. Opt. Soc. Am. B 31 (2014) 1410–1414.
[25] F.R. Hu, N.N. Xu, W.M. Wang, Y.E. Wang, W.T. Zhang, J.G. Han, W.L. Zhang, A dynamically tunable terahertz metamaterial absorber based on an electrostatic MEMS actuator and electrical dipole resonator array, J. Micromech. Microeng. 26 (2016) 025006.
[26] F.R. Hu, Y.X. Qian, Z. Li, J.H. Niu, K. Nie, X.M. Xiong, W.T. Zhang, Z.Y. Peng, Design of a tunable terahertz narrowband metamaterial absorber based on an electrostatically actuated MEMS cantilever and split ring resonator array, J. Opt. 15 (2013) 055101.
[27] N. Liu, H.C. Guo, L.W. Fu, S. Kaiser, H. Schweizer, H. Giessen, Three-dimensional photonic metamaterials at optical frequencies, Nat. Mater. 7 (2008) 31–37.
[28] C.C. Chen, A. Ishikawa, Y.H. Tang, M.H. Shiao, D.P. Tsai, T. Tanaka, Uniaxial-isotropic metamaterials by three-dimensional split-ring resonators, Adv. Opt. Mater. 3 (2015) 44–48.
[29] P. Pitchappa, M. Manjappa, H.N.S. Krishnamoorthy, Y.H. Chang, C.K. Lee, R. Singh, Bidirectional reconfiguration and thermal tuning of microcantilever metamaterial device operating from 77 K to 400 K, Appl. Phys. Lett. 111 (2017) 261101.
[30] X.H. Li, T.Y. Yang, W.Q. Zhu, X.G. Li, Continuously tunable terahertz metamaterial employing a thermal actuator, Microsyst. Technol. 19 (2013) 1145–1151.
[31] B.L. Davis, M.I. Hussein, Nanophononic metamaterial: thermal conductivity reduction by local resonance, Phys. Rev. Lett. 112 (2014) 055505.
[32] L.W. Martin, A.M. Rappe, Thin-film ferroelectric materials and their applications, Nat. Rev. Mater. 2 (2016) 16087.
[33] N. Maa, Y. Yang, Enhanced self-powered UV photoresponse of ferroelectric $BaTiO_3$ materials by pyroelectric effect, Nano Energy 40 (2017) 352–359.
[34] J.G. Han, A. Lakhtakia, Semiconductor split-ring resonators for thermally tunable terahertz metamaterials, J. Mod. Opt. 56 (2009) 554–557.
[35] Z.Q. Lin, F. Wang, M. Wang, L. Zhang, S.Y. Feng, G.J. Gao, S.K. Wang, C.L. Yu, L.L. Hu, Maintaining broadband gain in a Nd3+/Yb3+ co-doped silica fiber amplifier via dual-laser pumping, Opt. Lett. 43 (2018) 3361–3364.
[36] C.Y. Chen, C.L. Pan, C.F. Hsieh, Y.F. Lin, R.P. Pan, Liquid-crystal-based terahertz tunable Lyot filter, Appl. Phys. Lett. 88 (2006) 101107.
[37] R.J. Ma, Z.Y. Zhang, K. Tong, D. Huber, R. Kornbluh, Y.S. Ju, Q.B. Pei, Highly efficient electrocaloric cooling with electrostatic actuation, Science 357 (2017) 1130–1134.
[38] Y.S. Lin, Y. Qian, F. Ma, Z. Liu, P. Kropelnicki, C. Lee, Development of stress-induced curved actuators for a tunable THz filter based on double split-ring resonators, Appl. Phys. Lett. 102 (2013) 111908.
[39] J. Kischkat, S. Peters, B. Gruska, M. Semtsiv, M. Chashnikova, M. Klinkmüller, O. Fedosenko, S. Machulik, A. Aleksandrova, G. Monastyrskyi, Y. Flores, W.T. Masselink, Mid-infrared optical properties of thin films of aluminum oxide, titanium dioxide, silicon dioxide, aluminum nitride, and silicon nitride, Appl. Opt. 51 (2017) 6789–6798.